Nano Research 2017, 10(4): 1302–1312
DOI 10.1007/s12274-016-1416-z
Research Article
ISSN 1998-0124
CN 11-5974/O4

Enhancing both selectivity and coking-resistance of a single-atom Pd_1/C_3N_4 catalyst for acetylene hydrogenation

Xiaohui Huang[1,§], Yujia Xia[1,§], Yuanjie Cao[2], Xusheng Zheng[2], Haibin Pan[2], Junfa Zhu[2], Chao Ma[3], Hengwei Wang[1], Junjie Li[1], Rui You[1], Shiqiang Wei[2], Weixin Huang[1,3], and Junling Lu[1] (✉)

[1] *Department of Chemical Physics, iChEM, CAS Key Laboratory of Materials for Energy Conversion, University of Science and Technology of China, Hefei 230026, China*
[2] *National Synchrotron Radiation Laboratory, University of Science and Technology of China, Hefei 230029, China*
[3] *Hefei National Laboratory for Physical Sciences at the Microscale, University of Science and Technology of China, Hefei 230026, China*
[§] *These authors contributed equally to this work.*

Received: 11 November 2016
Revised: 9 December 2016
Accepted: 12 December 2016

KEYWORDS
single-atom catalyst,
Pd catalyst,
atomic layer deposition,
acetylene hydrogenation,
C_3N_4,
selectivity,
coke formation,
support effect

ABSTRACT

Selective hydrogenation is an important industrial catalytic process in chemical upgrading, where Pd-based catalysts are widely used because of their high hydrogenation activities. However, poor selectivity and short catalyst lifetime because of heavy coke formation have been major concerns. In this work, atomically dispersed Pd atoms were successfully synthesized on graphitic carbon nitride (g-C_3N_4) using atomic layer deposition. Aberration-corrected high-angle annular dark-field scanning transmission electron microscopy (HAADF-STEM) confirmed the dominant presence of isolated Pd atoms without Pd nanoparticle (NP) formation. During selective hydrogenation of acetylene in excess ethylene, the g-C_3N_4-supported Pd NP catalysts had strikingly higher ethylene selectivities than the conventional Pd/Al_2O_3 and Pd/SiO_2 catalysts. *In-situ* X-ray photoemission spectroscopy revealed that the considerable charge transfer from the Pd NPs to g-C_3N_4 likely plays an important role in the catalytic performance enhancement. More impressively, the single-atom Pd_1/C_3N_4 catalyst exhibited both higher ethylene selectivity and higher coking resistance. Our work demonstrates that the single-atom Pd catalyst is a promising candidate for improving both selectivity and coking-resistance in hydrogenation reactions.

1 Introduction

Hydrogenation reactions are widely performed in industrial catalytic processes for chemical upgrading. Therein, Pd-based catalysts are often used because of their high hydrogenation activities. Nonetheless, there have been two major long-term concerns regarding this type of catalytic processes: (1) poor selectivity, especially at high conversions, and (2) severe coke formation, which could cause quick catalyst deactivation

Address correspondence to junling@ustc.edu.cn

by blocking catalytically active sites [1–3]. Tremendous efforts have been devoted to improving the catalyst selectivity and durability.

Selective hydrogenation of acetylene or dienes is an industrially important reaction to remove trace amounts of alkynes or dienes from alkene streams [4–7]; adding a second metal [8–14] or applying an oxide overcoating [15–18] were the most frequently adopted methods to improve the Pd catalyst selectivity. Therein, the electronic properties of the Pd nanoparticles (NPs) were modified, and the continuous Pd surface ensembles were divided into much smaller ones by the second metal component or porous oxide overcoat. A single-atom alloy (SAA) catalyst represents one ultimate case of Pd-based bimetallic catalysts, in which Pd is usually present in low concentration and individually disperses on the second metal. For instance, Flytzani-Stephanopoulos and co-workers reported that single Pd atoms alloyed with Cu (111) surfaces were able to activate molecular H_2, rendering the alloy surfaces much more efficient for selective hydrogenation of styrene and acetylene than the corresponding monometallic Pd and Cu systems [19, 20]. Zhang et al. reported that Au- or Ag-alloyed Pd single atoms had significantly higher selectivities than an analogous monometallic Pd catalyst [21, 22]. They further showed that a PdZn intermetallic nanostructure with Pd–Zn–Pd ensembles was both highly active and selective for semi-hydrogenation of acetylene to ethylene [23]. Similar to SAAs, single-atom Pd catalysts also show a higher selectivity in hydrogenation reactions than Pd NP catalysts [24, 25]. Recently, we demonstrated an excellent single-atom Pd_1/graphene catalyst performance by showing about 100% butene selectivity at 95% conversion under mild reaction conditions (50 ℃) for selective hydrogenation of 1,3-butadiene [25].

In addition, catalyst supports have large effects on the catalyst performance. For instance, Datye et al. reported that a carbon-supported Pd catalyst yielded a higher selectivity to ethylene at high acetylene conversions than that provided by oxide-supported Pd catalysts [26]. However, the selectivity improvement was less than 30% at conversions above 80%. Panpranot et al. showed that the use of mixed-phase Al_2O_3 with approximately 64% of the alpha-phase provided significant improvements for both acetylene conversion and ethylene selectivity [27]. Bertolini et al. also reported that the catalyst deactivation behavior strongly depended on the nature of the support [28], where the activities of the Pd/SiO_2 and Pd/Si_3N_4 catalysts decreased rather rapidly in the first few hours, but the Pd/Al_2O_3 and Pd/SiC catalysts continuously lost their activity with time, even after 20 h on the reaction stream. Graphite-like carbon nitride (g-C_3N_4) based on tri-s-triazine (heptazine) units has received much attention for photocatalysis research because of its low cost, good stability, and excellent optical and electronic properties [29]. However, the use of g-C_3N_4 as a catalyst support has been relatively less reported [30]. Recently, López and co-workers demonstrated that isolated Pd atoms could be confined into the six-fold cavities of g-C_3N_4 in a stable manner, enabling the design of a single-site Pd catalyst for hydrogenation of alkynes and nitroarenes [24].

In this work, we first synthesized a single-atom Pd_1/C_3N_4 catalyst using atomic layer deposition (ALD), which relies on self-limiting binary surface reactions between gaseous precursors and the substrate [31, 32]. Moreover, four different Pd NP catalysts on g-C_3N_4, Al_2O_3, and SiO_2 supports were synthesized using different methods to compare the support effect. The g-C_3N_4-supported Pd NP catalyst had remarkably higher ethylene selectivities at high acetylene conversions than the Pd/Al_2O_3 and Pd/SiO_2 catalysts for selective hydrogenation of acetylene in excess ethylene. More interestingly, the single-atom Pd_1/C_3N_4 catalyst exhibited superior catalytic performances, including higher ethylene selectivity and higher coking-resistance over the g-C_3N_4-supported Pd NP catalysts.

2 Experimental section

2.1 Graphitic C_3N_4 support synthesis

Bulk g-C_3N_4 was synthesized by a thermal treatment of urea [33]. Typically, 10 g of urea powder was placed in an alumina crucible with a cover, slowly heated to 550 ℃ at a rate of 0.5 ℃·min^{-1} in a muffle furnace, and maintained at this temperature for 3 h. After cooling to room temperature, ~600 mg of bulk g-C_3N_4 was obtained. Then, 100 mg of the as-prepared bulk g-C_3N_4 was added to a 300-mL mixed solution of isopropanol

and water, with a volume ratio of 3:2, followed by 20 min of sonication. The mixture was then sealed in a Teflon-lined autoclave at 120 ℃ under autogenous pressure for 24 h. The resulting product was dried at 80 ℃ overnight to obtain the g-C_3N_4 support [34].

2.2 Pd/C_3N_4 catalyst synthesis

Pd ALD was performed using a viscous flow reactor (GEMSTAR-6™ Benchtop ALD, Arradiance) at 150 ℃ using palladium hexafluoroacetylacetate ($Pd(hfac)_2$, Sigma-Aldrich, 99.9%) and formalin (Aldrich, 37% HCHO and 15% CH_3OH in aqueous solution) [35, 36]. Ultrahigh purity N_2 (99.999%) was used as a carrier gas at a flow rate of 200 mL·min^{-1}. The $Pd(hfac)_2$ precursor container was heated to 65 ℃ to reach a sufficient vapor pressure. The chamber was heated to 150 ℃, and the inlet manifold was held at 115 ℃ to avoid precursor condensation. The timing sequence was 120, 120, 60, and 120 s for $Pd(hfac)_2$ exposure, N_2 purge, formalin exposure, and N_2 purge, respectively. One cycle and ten cycles of Pd ALD were performed on g-C_3N_4 at 150 ℃ to obtain a single-atom Pd_1/C_3N_4 catalyst and a Pd NP catalyst (Pd/C_3N_4-NP(ALD)), respectively.

We synthesized another Pd/C_3N_4 NP catalyst using the wet-impregnation (WI) method (Pd/C_3N_4-NP(WI)) [24]. Briefly, 0.94 mL of $PdCl_2$ (0.02 mol·L^{-1}) and 44 mg of citric acid (Sinopharm Chemical Reagent Co., Ltd., ≥99.5%) were dissolved into 50 mL of water to form a Pd-citric acid solution. Next, 100 mg of g-C_3N_4 was added to the solution and mixed. An aqueous solution of $NaBH_4$ (0.016 mol·L^{-1}, 10 mL) was then added to this mixture and stirred for 8 h at 60 ℃. Then, the mixture was separated by filtration, followed by a thorough washing with deionized water. The obtained material was then dried overnight in a vacuum oven at 50 ℃. Finally, the dried material was calcined in 10% O_2 in He at 300 ℃ for 2 h, and reduced at 200 ℃ for another 0.5 h in 10% H_2 in He to obtain the Pd/C_3N_4-NP(WI) catalyst.

2.3 Pd/Al_2O_3 and Pd/SiO_2 catalyst synthesis

Pd/Al_2O_3 and Pd/SiO_2 catalysts were also synthesized to study the support effect. The Pd/Al_2O_3 catalyst was synthesized by one cycle of Pd ALD on spherical alumina powder (NanoDur, 99.5%, Alfa Aesar) at 150 ℃ using the same timing sequence. Meanwhile, the Pd/SiO_2 catalyst was synthesized by the WI method [37]. Therein, 52 mg of palladium acetylacetonate (Sinopharm Chemical Reagent Co., Ltd.) was first dissolved into 50 mL of acetylacetone to prepare a 1.04 mg·mL^{-1} impregnation Pd solution. Next, 30.2 mL of the Pd solution and 1 g of spherical SiO_2 were co-added to a 100-mL flask and stirred at 25 ℃ for 24 h, during which the solvent was slowly evaporated under stirring. The obtained solid was further dried at 110 ℃ overnight and then calcined at 500 ℃ under 10% O_2 in He for 3 h, followed by a reduction step at 250 ℃ under 10% H_2 in Ar for another 2 h to obtain the Pd/SiO_2 catalyst.

2.4 Characterization

The Pd loadings in these samples were determined using an inductively coupled plasma atomic emission spectrometer (ICP-AES). The morphology was investigated using aberration-corrected high-angle annular dark-field scanning transmission electron microscopy (HAADF-STEM) at 200 kV (JEOL-2010F, University of Science and Technology of China (USTC)). The Pd particle size distribution was obtained by counting more than 200 Pd NPs from the HAADF-STEM images at different locations using the ImageJ software.

In-situ X-ray photoemission spectroscopy (XPS) measurements were performed at the photoemission end-station at the BL10B beamline, National Synchrotron Radiation Laboratory (NSRL) in Hefei, China. Briefly, the beamline is connected to a bending magnet and covers photon energies from 60 to 1,000 eV. The end-station consists of four chambers: (1) analysis chamber, (2) preparation chamber, (3) quick sample load-lock chamber, and (4) high-pressure reactor. The analysis chamber, with a base pressure of $<2 \times 10^{-10}$ torr, is connected to the beamline and equipped with a VG Scienta R3000 electron energy analyzer and a twin-anode X-ray source. The high-pressure reactor houses a reaction cell where the samples can be treated with different gases up to 20 bar and simultaneously heated up to 650 ℃. After sample treatment, the reactor can be pumped down to high vacuum ($<10^{-8}$ torr) for sample transfer. In the current work, a sample

was first treated with 10% H_2 in Ar at 150 ℃ for 0.5 h in the high-pressure reactor. Next, the sample was transferred to the analysis chamber for XPS measurements in the Pd 3d region without exposure to air.

2.5 Reaction test

Selective hydrogenation of acetylene in excess ethylene was conducted in a fixed-bed flow reactor. The total flow rate was kept at 50 mL·min^{-1}. The catalyst amount was 50 mg, which was diluted with 1 g of 60–80 mesh quartz chips. Prior to the reaction test, all catalysts were reduced in 10% H_2 in Ar at 150 ℃ for 0.5 h. Then the feed gas, which consisted of 0.5% acetylene, 1% H_2, and 25% ethylene with Ar as the balance gas, was introduced to the reactor to start the reaction. The reaction products were analyzed using an online gas chromatograph equipped with a flame ionization detector and a capillary column (ValcoPLOT VP-Alumina-KCl, 50 m × 0.53 mm). The acetylene conversion and ethylene selectivity were calculated as follows

$$C_2H_2 \text{ conversion} = \left(\frac{[C_2H_2]_{in} - [C_2H_2]_{out}}{[C_2H_2]_{in}}\right) \times 100\% \quad (1)$$

$$C_2H_4 \text{ selectivity} = \left(1 - \frac{[C_2H_6]_{out} - [C_2H_6]_{in}}{[C_2H_2]_{in} - [C_2H_2]_{out}}\right) \times 100\% \quad (2)$$

3 Results and discussion

3.1 Morphology of Pd catalysts

The Pd loadings of the Pd catalysts are listed in Table 1. They were 0.5% and 0.3% after one Pd ALD cycle on the g-C_3N_4 (Pd_1/C_3N_4) and Al_2O_3 supports (Pd/Al_2O_3), respectively. The Pd loading increased to 3.5% after ten cycles of Pd ALD on g-C_3N_4 (Pd/C_3N_4-NP(ALD)). The Pd loadings were 1.8% and 1.0% on Pd/C_3N_4-NP(WI) and Pd/SiO_2, respectively.

Table 1 Pd loadings in the Pd catalysts

Catalysts	Pd loading (wt.%)
Pd_1/C_3N_4	0.5
Pd/C_3N_4-NP(ALD)	3.5
Pd/C_3N_4-NP(WI)	1.8
Pd/Al_2O_3	0.3
Pd/SiO_2	1.0

Aberration-corrected HAADF-STEM measurements show that a high density of atomically dispersed Pd atoms formed after one cycle of Pd ALD on g-C_3N_4 at 150 ℃; neither the Pd NPs nor the subnanometer clusters were observed at low or high magnifications (Figs. 1(a)–1(d)). This is quite different than that observed for Pd ALD on oxide surfaces, where Pd NPs are often formed [35, 36, 38]. Indeed, Pd NPs with particle sizes of 2.8 ± 0.7 nm were formed on the Al_2O_3 support under identical ALD conditions (Fig. 1(e)).

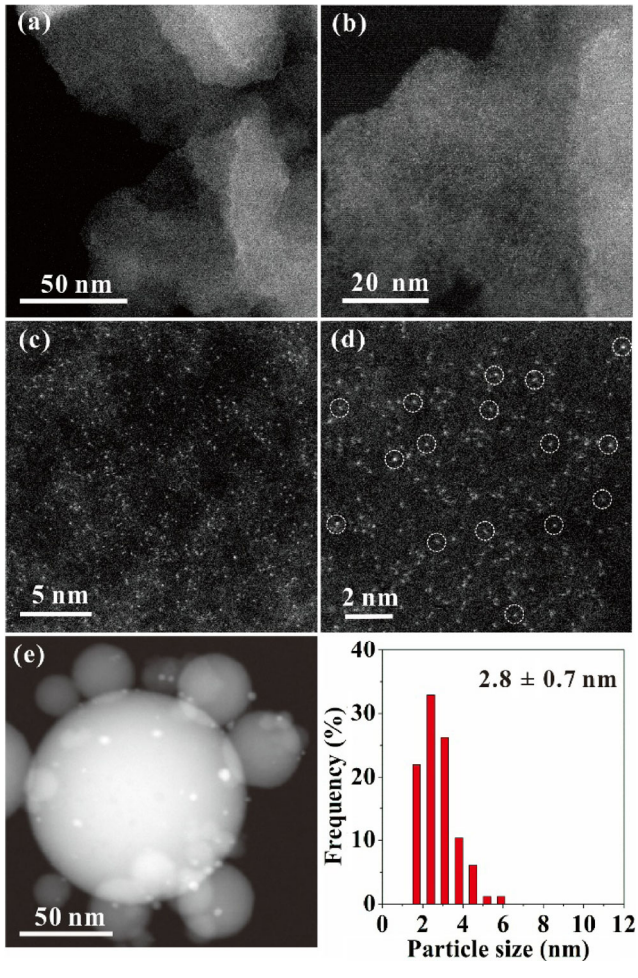

Figure 1 Aberration-corrected HAADF-STEM images of the single-atom Pd_1/C_3N_4 catalyst at different magnifications ((a)–(d)) and the Pd/Al_2O_3 catalyst, as well as its corresponding particle size distribution (e). The representative Pd single atoms in (d) are highlighted by white circles.

Recently, López and co-workers demonstrated that single Pd atoms anchored at the cavities of g-C_3N_4 were very stable in hydrogenation reactions [24]. Du et al. used density functional theory calculations to show that Pd atoms can strongly bond to the six-fold cavity with a calculated binding energy of −2.17 eV [39]. Therefore, the formation of isolated Pd atoms instead of Pd NPs on g-C_3N_4 might be attributed to the presence of six-fold cavities, which provide strong anchor sites for stabilizing isolated metal atoms during ALD synthesis at elevated temperatures. During $Pd(hfac)_2$ exposure, $Pd(hfac)_2$ might dissociatively chemisorb at the six-fold cavities of g-C_3N_4 by forming Pd-hfac* and hfac* surface species, as shown in the schematic model in Fig. 2. Next, the hfac* ligand is removed by the formaldehyde reducing agent, and Pd single atoms are formed on the six-fold cavities; this is similar to depositing Pd on the surface of Au nanoparticles [37]. Nevertheless, the contributions of impurities, such as the oxygen-functional groups introduced during g-C_3N_4 synthesis, to Pd nucleation cannot be ruled out [25]. The detailed mechanism for the growth of Pd single atoms on g-C_3N_4 requires further investigation.

When ten cycles of Pd ALD were performed on g-C_3N_4, the size of the Pd NPs increased to about 6.0 ± 1.2 nm (Fig. 3(a)), similar to that for Pd ALD on active carbon [40, 41]. In addition, we also synthesized two additional Pd NP catalysts on g-C_3N_4 and SiO_2 supports for comparison. The Pd/C_3N_4-NP(WI) catalyst showed a very narrow Pd particle size distribution with an average size of 2.5 ± 0.3 nm (Fig. 3(b)), while the Pd/SiO_2 catalyst showed a Pd particle size of 5.4 ± 1.6 nm (Fig. 3(c)).

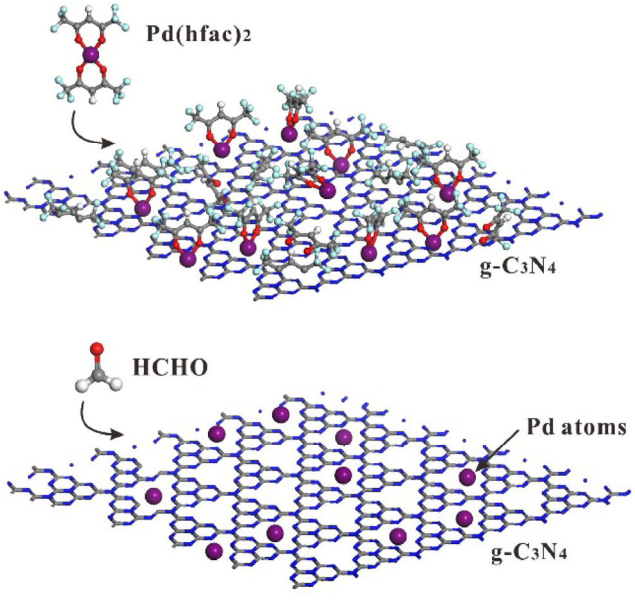

Figure 2 Schematic illustration of a single-atom Pd_1/C_3N_4 catalyst synthesized by Pd ALD on pristine g-C_3N_4.

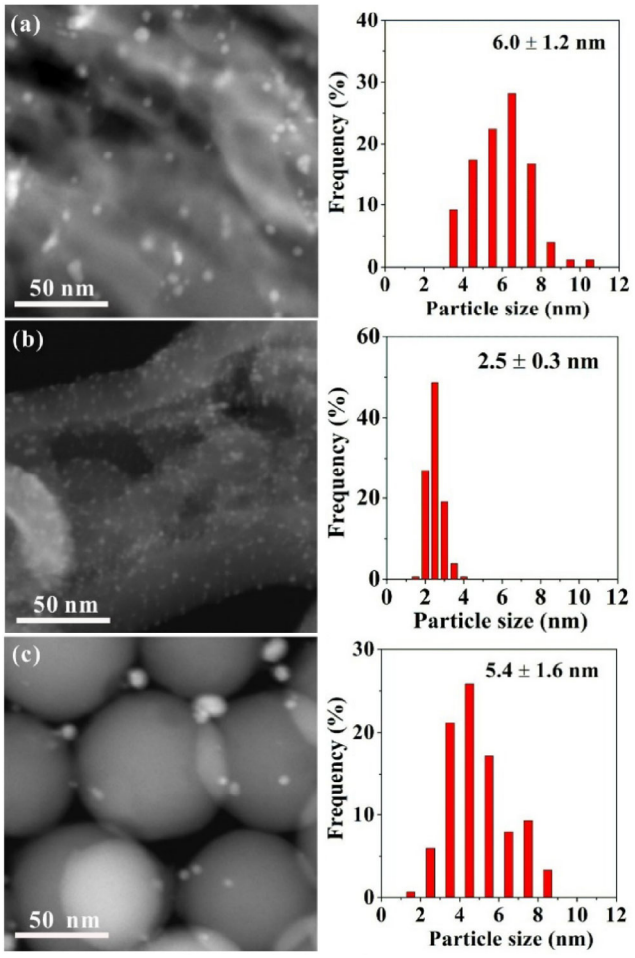

Figure 3 STEM images (left) and particle size distributions (right) for (a) Pd/C_3N_4-NP(ALD), (b) Pd/C_3N_4-NP(WI), and (c) Pd/SiO_2.

3.2 Electronic properties of Pd catalysts

The electronic properties of Pd single atoms or NPs in Pd_1/C_3N_4, Pd/C_3N_4-NP(ALD), and Pd/SiO_2 were selectively investigated by *in-situ* XPS in the Pd 3d region. As shown in Fig. 4(a), the Pd $3d_{5/2}$ binding energy on the single-atom Pd_1/C_3N_4 catalyst was mainly located at 336.7 eV, with a pronounced shoulder at 338.3 eV. Deconvolution of the XPS spectrum showed

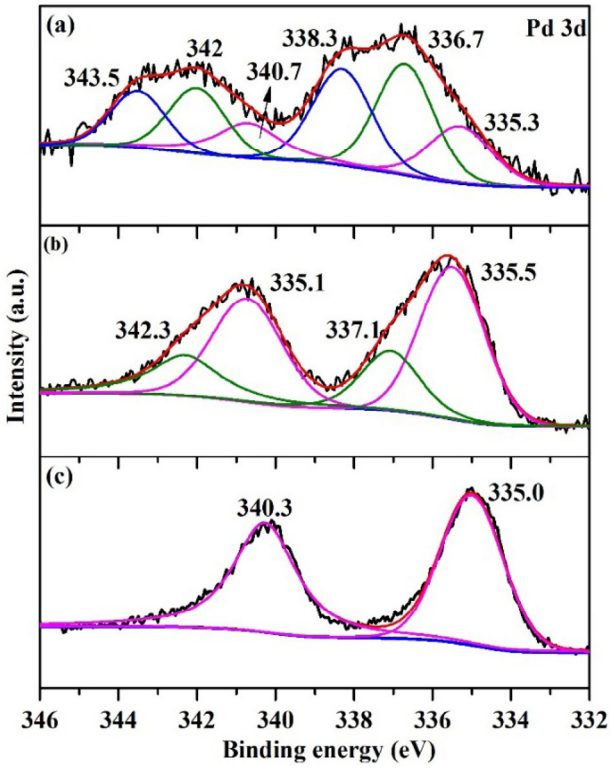

Figure 4 Pd 3d XPS spectra of (a) Pd_1/C_3N_4, (b) Pd/C_3N_4-NP(ALD), and (c) Pd/SiO_2.

35% Pd^{4+}, 39% Pd^{2+}, and 26% metallic Pd, according to the reported assignments [42]. Atomically dispersed Pd atoms in the Pd_1/C_3N_4 sample were predominantly positively charged. However, different local chemical environments around the Pd atoms, such as defects and impurities, might cause different Pd single atom charges [34, 43]. This result is consistent with our previous observation where we found that Pd single atoms on reduced graphene were mainly in the 2+ state [25]. In addition, theoretical calculations also demonstrated that Pd atoms anchored on the six-fold cavities are positively charged [39]. On the 6.0 nm Pd/C_3N_4-NP(ALD) sample, the Pd $3d_{5/2}$ peak was mainly located at 335.5 eV, along with a smaller shoulder at 337.1 eV (Fig. 4(b)), which was about 68% Pd^0 and 32% Pd^{2+}. The metallic Pd component was still considerably shifted to a higher binding energy compared to that for bulk Pd [44]. While on the 5.4-nm Pd/SiO_2 sample, Pd was completely reduced to the metallic state, and the Pd $3d_{5/2}$ peak was located at 335.0 eV (Fig. 4(c)), which is very close to the value for the bulk Pd metal [44]. Clearly, a considerable charge transfer from Pd to g-C_3N_4 occurred on the g-C_3N_4-supported Pd single atoms or NP samples, in line with the case of metal on nitrogen-doped carbon [45, 46]. The charge transfer is likely attributed to the exchange-transfer mechanism, where the increased number of electrons on the Pd d_{xz}+d_{yz} and N p_z orbitals is largely compensated by electron depletion on the Pd d_z^2 and N p_x+p_y orbitals [47, 48], which clearly indicates a strong interaction between the lone-pair electrons of the neighboring pyridinic nitrogen atoms and the isolated Pd atoms.

3.3 Catalytic performance

The catalytic performances of these Pd samples were evaluated for the selective hydrogenation of acetylene in excess ethylene. As shown in Fig. 5(a), 100% acetylene conversion was reached on the 5.4-nm Pd/SiO_2 catalyst near 70 ℃. The 2.8-nm Pd/Al_2O_3 catalyst required a much higher temperature (130 ℃) for complete conversion, although its initial activity was close to that of Pd/SiO_2. Such behavior on Pd/Al_2O_3 is likely due to more pronounced coke formation because heavier coke was usually formed on smaller Pd NPs in hydrogenation reactions owing to a larger fraction of low-coordination sites [49]. Meanwhile, we also noticed that Pd/C_3N_4-NP(ALD), with an average particle size of 6.0 nm, was more active than the 2.5-nm Pd/C_3N_4-NP(WI) catalyst. This is not surprising because the ALD catalyst had a significantly higher Pd loading (Table 1). However, larger Pd NPs for Pd/C_3N_4-NP(ALD) might also contribute to the high activity, where larger Pd NPs often show a higher activity in hydrogenation reactions [49–52]. Interestingly, the activities of Pd/C_3N_4-NP(ALD) and Pd/C_3N_4-NP(WI) were generally higher than that of the Pd NPs supported on conventional Al_2O_3 and SiO_2 supports, regardless of the Pd particle size. Higher Pd loadings in Pd/C_3N_4-NP(ALD) and Pd/C_3N_4-NP(WI) can certainly contribute to the higher activity. While the electronic effect induced by the g-C_3N_4 support (according to our XPS results in Fig. 4) might also significantly contribute to the improved activity. The single-atom Pd_1/C_3N_4 catalyst showed a considerably lower activity, and the acetylene conversion was only about 13% at 80 ℃, and 100% conversion was achieved at 115 ℃.

Figure 5(b) illustrates the ethylene selectivity as a function of acetylene conversion over these Pd catalysts.

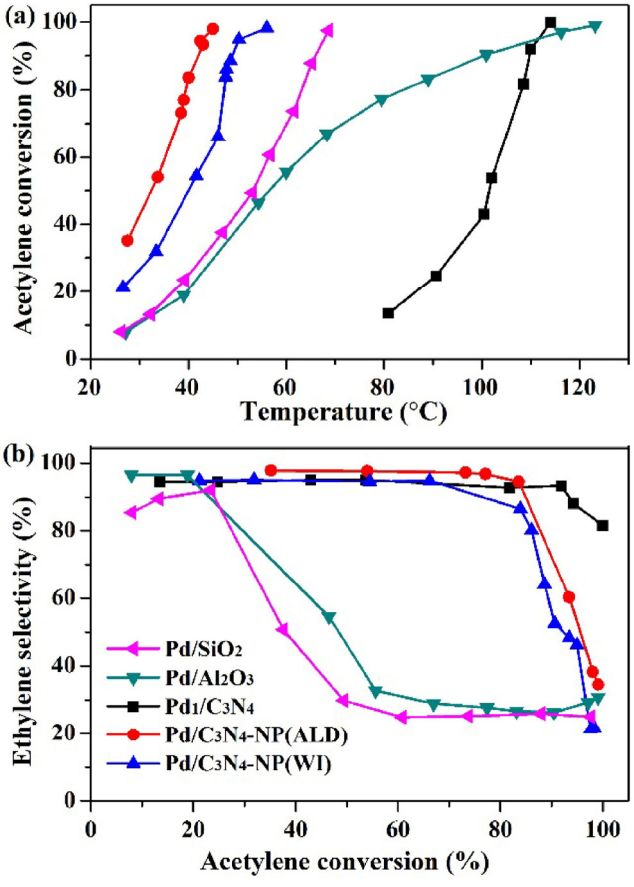

Figure 5 (a) Acetylene conversion as a function of reaction temperature on the various Pd catalysts in selective hydrogenation of acetylene in excess ethylene. (b) Ethylene selectivity as a function of acetylene conversion. The legends in (b) also apply to (a). Reaction conditions: 0.5% acetylene, 1% H_2, 25% ethylene balanced in Ar; space velocity = 60,000 $mL \cdot g^{-1} \cdot h^{-1}$; pressure = 0.1 MPa.

When the conversion was above 20%, the ethylene selectivity dropped rapidly on both the Pd/Al_2O_3 and Pd/SiO_2 catalysts, which is consistent with our previous work [17] and Ref. [53]. However, we surprisingly found that the ethylene selectivity was preserved at higher conversions on the two g-C_3N_4-supported Pd NP catalysts, regardless of the synthesis methods. At a conversion of 84%, the ethylene selectivities were about 94% and 86% on Pd/C_3N_4-NP(ALD) and Pd/C_3N_4-NP(WI), respectively, which were both much higher than that of the Pd/Al_2O_3 (26%) and Pd/SiO_2 (26%) catalysts. The enormous improvement in the ethylene selectivity on the two g-C_3N_4-supported Pd NP catalysts compared to Pd/Al_2O_3 and Pd/SiO_2 was significantly greater than the selectivity improvement observed on the carbon-supported Pd catalyst, where the ethylene selectivity was less than 30% at conversions above 80% [26]. The selectivity improvement here is certainly not related to the Pd particle size because the two g-C_3N_4-supported Pd NP catalysts with smaller (2.5 nm) and larger (6.0 nm) Pd particle sizes both showed a similar selectivity enhancement. Considerable charge transfer from the Pd NPs to g-C_3N_4 likely plays an important role, according to our XPS results in Fig. 4.

The single-atom Pd_1/C_3N_4 catalyst exhibited even higher ethylene selectivity at high conversions, compared to that for Pd/C_3N_4-NP(ALD) and Pd/C_3N_4-NP (WI). An ethylene selectivity of 83% was achieved on Pd_1/C_3N_4 at 99% conversion (Fig. 5(b)). In contrast, the ethylene selectivity dropped quickly above 84% conversion, and it was 35% and 22% on Pd/C_3N_4-NP(ALD) and Pd/C_3N_4-NP(WI), respectively, at 99% conversion. A remarkably higher selectivity was achieved on single Pd atoms than Pd NPs, which is consistent with our previous work, where we found that single-atom Pd_1/graphene catalysts had a much higher butene selectivity in selective hydrogenation of 1,3-butadiene [25]. On a continuous Pd surface, acetylene partly converts to ethylidyne after adsorption. Sandell reported that it forms an ordered $(\sqrt{3} \times \sqrt{3})$ R30° structure [54]. These adsorbates divide the Pd surface into so-called "A" and "E" sites, where the "A" sites adsorb acetylene and hydrogen but do not adsorb ethylene because of steric hindrance [3, 55]. A higher ethylene packing density is expected on a single-atom Pd catalyst; thus, Pd single atoms represent only the "A" sites and remarkably improve the ethylene selectivity.

We further examined the durability of the Pd/C_3N_4-NP(WI) and Pd_1/C_3N_4 catalysts at 55 °C for 100 h, as shown in Fig. 6. On Pd/C_3N_4-NP(WI), the initial conversion was 53% after introducing the reaction gas to the reactor for 5 min; it then increased to a maximum of 82% after about 7 h (Fig. 6(a)). Then, the conversion decreased quickly and stabilized at 47%. The activity decrease between the maximum, and the stabilized conversion was 35%. Meanwhile, the selectivity decreased from 95% to 87% after the 100 h long-term test. In addition, a reasonable amount of liquid green

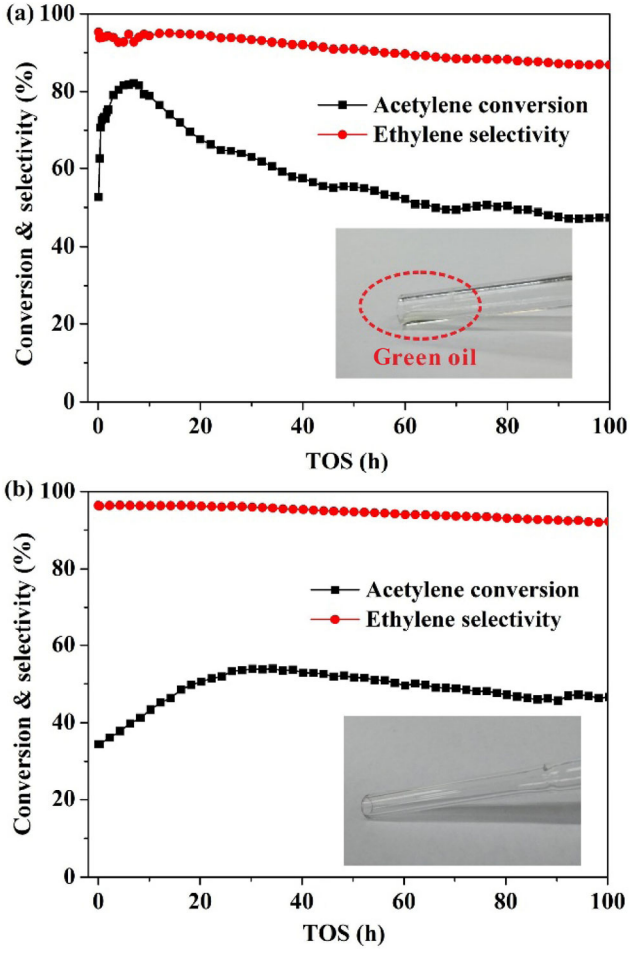

Figure 6 Durability test on (a) Pd/C_3N_4-NP(WI) and (b) Pd_1/C_3N_4 in the selective hydrogenation of acetylene in excess ethylene for 100 h at about 55 ˚C. The insets are the photographs of the reactor outlet after the long-term stability test; considerable green oil was formed when using the Pd/C_3N_4-NP(WI) catalyst. Reaction conditions: 0.5% acetylene, 1% H_2, 25% ethylene balanced in Ar; space velocity = 60,000 $mL \cdot g^{-1} \cdot h^{-1}$; pressure = 0.1 MPa.

oil formed in the reactor outlet after the long-term test (inset of Fig. 6(a)). The single-atom Pd_1/C_3N_4 catalyst exhibited an initial conversion of 35% after 5 min and reached a maximum of 54% after 30 h (Fig. 6(b)). Then, the conversion slowly decreased and stabilized at 46%. The activity drop was 8% from the maximum, much less than that on Pd/C_3N_4-NP(WI). The selectivity decreased slightly from 96% to 92%. In this case, the reactor outlet was rather clean, and green oil was not observed. Therefore, our results clearly imply that coke formation on the single-atom Pd_1/C_3N_4 catalyst was largely suppressed compared to that for the Pd NP catalyst. The improved coking-resistance on Pd single atoms is likely due to the geometric effect, on which the multiple adjacent adsorption sites that are required for polymerization of acetylene or ethylene to form green oil (or coke) [3] are not available, rendering less opportunities for coke formation than on an extended Pd NP surface.

Figure 7 shows the morphology of the single-atom Pd_1/C_3N_4 catalyst after the long-term durability test at 55 ˚C for 100 h. A few Pd NPs with a particle size of ~8 nm were observed. In addition, a large number of isolated Pd atoms survived (Figs. 7(b)–7(d)). The aggregation of Pd atoms under these reaction conditions is likely induced by strong metal-reactant

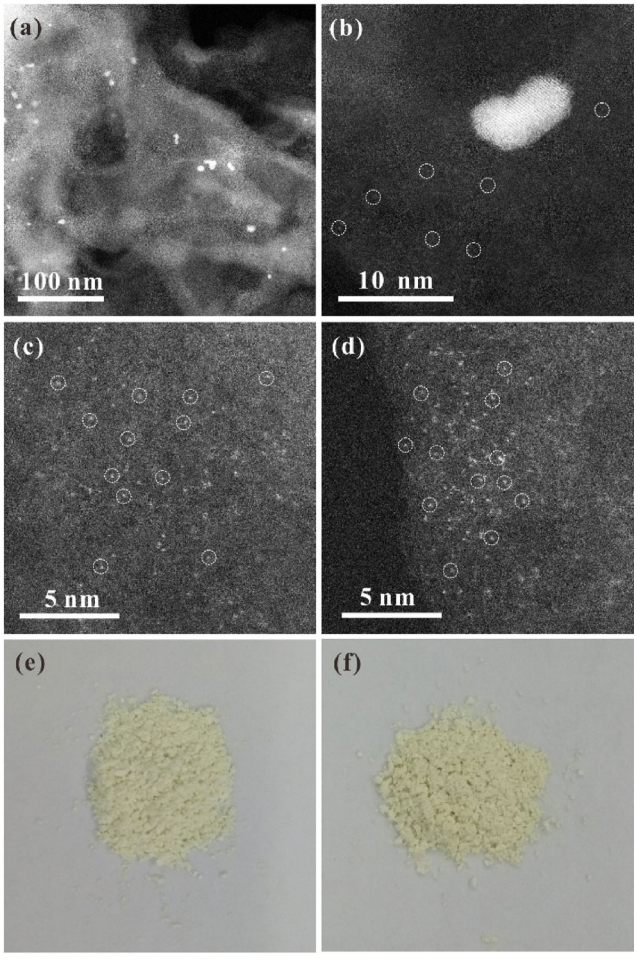

Figure 7 (a)–(d) Representative aberration-corrected HAADF-STEM images of the single-atom Pd_1/C_3N_4 catalyst after 100 h of reaction time on stream at about 55 ˚C. Some of the representative Pd single atoms in ((b)–(d)) are highlighted by white circles. Photographs of (e) as-prepared g-C_3N_4 and (f) the g-C_3N_4 support after reduction at 400 ˚C in 10% H_2 in Ar for 0.5 h.

interactions [56]. Consequently, the slight decrease in both activity and selectivity on the single-atom Pd_1/C_3N_4 catalyst, shown in Fig. 6(b), can be attributed to aggregation of Pd atoms because the number of Pd active sites was largely reduced by aggregation, and coking was further accelerated on the formed Pd NPs. These results imply that the single-atom Pd catalyst, in principle, is an ideal candidate for improving both the selectivity and coking-resistance in hydrogenation reactions once aggregation of Pd atoms was prevented. The g-C_3N_4 support itself is very stable under the current reaction conditions because no visible change in the color of g-C_3N_4 (light yellow) was observed, even after the high-temperature reduction at 400 °C in 10% H_2 in Ar for 0.5 h (Figs. 7(e) and 7(f)).

4 Conclusions

In conclusion, we successfully synthesized a single-atom Pd_1/C_3N_4 catalyst using the ALD method. HAADF-STEM confirmed the dominant presence of isolated Pd atoms without Pd NP formation. The six-fold cavities on g-C_3N_4 are likely the anchor sites for Pd atoms. In addition, four different Pd NP catalysts on g-C_3N_4, Al_2O_3, and SiO_2 supports were synthesized using different methods for investigating the support effect. In selective hydrogenation of acetylene in excess ethylene, it was very surprising to find that g-C_3N_4 supported Pd NP catalysts had both remarkably higher ethylene selectivities at high acetylene conversions and higher activities than that of the Pd/Al_2O_3 and Pd/SiO_2 catalysts, regardless of the Pd particle size. *In-situ* XPS measurements revealed that considerable charge transfer from Pd NPs to g-C_3N_4 likely plays an important role for the catalytic performance enhancement. Next, we compared the catalytic performance of g-C_3N_4-supported Pd NP catalysts with the single-atom Pd_1/C_3N_4 catalyst. Pd_1/C_3N_4 exhibited much higher ethylene selectivity than the Pd NP catalysts at near complete conversions, although the activity was lower. More importantly, the single-atom Pd_1/C_3N_4 catalyst demonstrated a high resistance to coke formation.

In brief, our results show that g-C_3N_4 has a high stability in either reducing or oxidizing environments at high temperatures and appears to be a very promising catalyst support for tailoring the electronic properties of metal NPs, thereby greatly enhancing the catalytic performance. Moreover, the findings provide strong evidence that a single-atom Pd catalyst, in principle, can be an ideal candidate for improving both selectivity and coking-resistance in hydrogenation reactions, once aggregations of Pd atoms are prevented.

Acknowledgements

This work was supported by the Thousand Talents Plan, the National Natural Science Foundation of China (Nos. 21473169, 21673215, and 51402283), the Fundamental Research Funds for the Central Universities (Nos. WK2060030017 and WK2060190026), and the startup funds from the University of Science and Technology of China. This work was also supported by Hefei Science Center (No. 2015HSC-UP010).

References

[1] Argyle, M. D.; Bartholomew, C. H. Heterogeneous catalyst deactivation and regeneration: A review. *Catalysts* **2015**, *5*, 145–269.

[2] Barbier, J. Deactivation of reforming catalysts by coking—A review. *Appl. Catal.* **1986**, *23*, 225–243.

[3] Borodziński, A.; Bond, G. C. Selective hydrogenation of ethyne in ethene-rich streams on palladium catalysts. Part 1. Effect of changes to the catalyst during reaction. *Catal. Rev.* **2006**, *48*, 91–144.

[4] Bos, A. N. R.; Westerterp, K. R. Mechanism and kinetics of the selective hydrogenation of ethyne and ethene. *Chem. Eng. Process.* **1993**, *32*, 1–7.

[5] Schbib, N. S.; García, M. A.; Gígola, C. E.; Errazu, A. F. Kinetics of front-end acetylene hydrogenation in ethylene production. *Ind. Eng. Chem. Res.* **1996**, *35*, 1496–1505.

[6] Zhang, Q. W.; Li, J.; Liu, X. X.; Zhu, Q. M. Synergetic effect of Pd and Ag dispersed on Al_2O_3 in the selective hydrogenation of acetylene. *Appl. Catal. A: Gen.* **2000**, *197*, 221–228.

[7] Osswald, J.; Giedigkeit, R.; Jentoft, R.; Armbruster, M.; Girgsdies, F.; Kovnir, K.; Ressler, T.; Grin, Y.; Schlogl, R. Palladium–gallium intermetallic compounds for the selective hydrogenation of acetylene: Part I: Preparation and structural investigation under reaction conditions. *J. Catal.* **2008**, *258*, 210–218.

[8] Crabb, E. M.; Marshall, R. Properties of alumina supported Pd-Fe and Pt-Fe catalysts prepared using surface organo-

metallic chemistry. *Appl. Catal. A: Gen.* **2001**, *217*, 41–53.

[9] El Kolli, N.; Delannoy, L.; Louis, C. Bimetallic Au–Pd catalysts for selective hydrogenation of butadiene: Influence of the preparation method on catalytic properties. *J. Catal.* **2013**, *297*, 79–92.

[10] Hou, R. J.; Ye, W. T.; Porosoff, M. D.; Chen, J. G.; Wang, T. F. Selective hydrogenation of 1,3-butadiene on Pd–Ni bimetallic catalyst: From model surfaces to supported catalysts. *J. Catal.* **2014**, *316*, 1–10.

[11] Verdier, S.; Didillon, B.; Morin, S.; Uzio, D. Pd-Sn/Al_2O_3 catalysts from colloidal oxide synthesis: II. Surface characterization and catalytic properties for buta-1,3-diene selective hydrogenation. *J. Catal.* **2003**, *218*, 288–295.

[12] Sarkany, A.; Zsoldos, Z.; Stefler, G.; Hightower, J. W.; Guczi, L. Promoter effect of Pd in hydrogenation of 1,3-butadiene over Co-Pd catalysts. *J. Catal.* **1995**, *157*, 179–189.

[13] Goetz, J.; Volpe, M. A.; Gigola, C. E.; Touroude, R. Low-loaded Pd-Pb/α-Al_2O_3 catalysts: Effect of alloying in the hydrogenation of buta-1,3-diene and hydrogenation and isomerization of butenes. *J. Catal.* **2001**, *199*, 338–345.

[14] Pattamakomsan, K.; Ehret, E.; Morfin, F.; Gélin, P.; Jugnet, Y.; Prakash, S.; Bertolini, J. C.; Panpranot, J.; Aires, F. J. C. S. Selective hydrogenation of 1,3-butadiene over Pd and Pd–Sn catalysts supported on different phases of alumina. *Catal. Today* **2011**, *164*, 28–33.

[15] Lee, D. C.; Kim, J. H.; Kim, W. J.; Kang, J. H.; Moon, S. H. Selective hydrogenation of 1,3-butadiene on TiO_2-modified Pd/SiO_2 catalysts. *Appl. Catal. A: Gen.* **2003**, *244*, 83–91.

[16] Yi, H.; Du, H. Y.; Hu, Y. L.; Yan, H.; Jiang, H. L.; Lu, J. L. Precisely controlled porous alumina overcoating on Pd catalyst by atomic layer deposition: Enhanced selectivity and durability in hydrogenation of 1,3-butadiene. *ACS Catal.* **2015**, *5*, 2735–2739.

[17] Ding, L. B.; Yi, H.; Zhang, W. H.; You, R.; Cao, T.; Yang, J. L.; Lu, J. L.; Huang, W. X. Activating edge sites on Pd catalysts for selective hydrogenation of acetylene via selective Ga_2O_3 decoration. *ACS Catal.* **2016**, *6*, 3700–3707.

[18] Kang, J. H.; Shin, E. W.; Kim, W. J.; Park, J. D.; Moon, S. H. Selective hydrogenation of acetylene on Pd/SiO_2 catalysts promoted with Ti, Nb and Ce oxides. *Catal. Today* **2000**, *63*, 183–188.

[19] Boucher, M. B.; Zugic, B.; Cladaras, G.; Kammert, J.; Marcinkowski, M. D.; Lawton, T. J.; Sykes, E. C. H.; Flytzani-Stephanopoulos, M. Single atom alloy surface analogs in $Pd_{0.18}Cu_{15}$ nanoparticles for selective hydrogenation reactions. *Phys. Chem. Chem. Phys.* **2013**, *15*, 12187–12196.

[20] Kyriakou, G.; Boucher, M. B.; Jewell, A. D.; Lewis, E. A.; Lawton, T. J.; Baber, A. E.; Tierney, H. L.; Flytzani-Stephanopoulos, M.; Sykes, E. C. H. Isolated metal atom geometries as a strategy for selective heterogeneous hydrogenations. *Science* **2012**, *335*, 1209–1212.

[21] Pei, G. X.; Liu, X. Y.; Wang, A. Q.; Li, L.; Huang, Y. Q.; Zhang, T.; Lee, J. W.; Jang, B. W. L.; Mou, C.-Y. Promotional effect of Pd single atoms on Au nanoparticles supported on silica for the selective hydrogenation of acetylene in excess ethylene. *New J. Chem.* **2014**, *38*, 2043–2051.

[22] Pei, G. X.; Liu, X. Y.; Wang, A. Q.; Lee, A. F.; Isaacs, M. A.; Li, L.; Pan, X. L.; Yang, X. F.; Wang, X. D.; Tai, Z. J. et al. Ag alloyed Pd single-atom catalysts for efficient selective hydrogenation of acetylene to ethylene in excess ethylene. *ACS Catal.* **2015**, *5*, 3717–3725.

[23] Zhou, H. R.; Yang, X. F.; Li, L.; Liu, X. Y.; Huang, Y. Q.; Pan, X. L.; Wang, A. Q.; Li, J.; Zhang, T. PdZn intermetallic nanostructure with Pd–Zn–Pd ensembles for highly active and chemoselective semi-hydrogenation of acetylene. *ACS Catal.* **2016**, *6*, 1054–1061.

[24] Vilé, G.; Albani, D.; Nachtegaal, M.; Chen, Z. P.; Dontsova, D.; Antonietti, M.; López, N.; Pérez-Ramírez, J. A stable single-site palladium catalyst for hydrogenations. *Angew. Chem., Int. Ed.* **2015**, *54*, 11265–11269.

[25] Yan, H.; Cheng, H.; Yi, H.; Lin, Y.; Yao, T.; Wang, C. L.; Li, J. J.; Wei, S. Q.; Lu, J. L. Single-atom Pd_1/graphene catalyst achieved by atomic layer deposition: Remarkable performance in selective hydrogenation of 1,3-butadiene. *J. Am. Chem. Soc.* **2015**, *137*, 10484–10487.

[26] Benavidez, A. D.; Burton, P. D.; Nogales, J. L.; Jenkins, A. R.; Ivanov, S. A.; Miller, J. T.; Karim, A. M.; Datye, A. K. Improved selectivity of carbon-supported palladium catalysts for the hydrogenation of acetylene in excess ethylene. *Appl. Catal. A: Gen.* **2014**, *482*, 108–115.

[27] Komhom, S.; Mekasuwandumrong, O.; Praserthdam, P.; Panpranot, J. Improvement of Pd/Al_2O_3 catalyst performance in selective acetylene hydrogenation using mixed phases Al_2O_3 support. *Catal. Commun.* **2008**, *10*, 86–91.

[28] Cervantes, G. G.; Aires, F. J. C. S.; Bertolini, J. C. Compared properties of Pd on thermo-conductor supports (SiC, Si_3N_4) and Pd on oxide supports (Al_2O_3, SiO_2) for the 1,3-butadiene hydrogenation reaction. *J. Catal.* **2003**, *214*, 26–32.

[29] Wang, X. C.; Blechert, S.; Antonietti, M. Polymeric graphitic carbon nitride for heterogeneous photocatalysis. *ACS Catal.* **2012**, *2*, 1596–1606.

[30] Gong, Y. T.; Li, M. M.; Li, H. R.; Wang, Y. Graphitic carbon nitride polymers: Promising catalysts or catalyst supports for heterogeneous oxidation and hydrogenation. *Green Chem.* **2015**, *17*, 715–736.

[31] Lu, J. L.; Elam, J. W.; Stair, P. C. Synthesis and stabilization of supported metal catalysts by atomic layer deposition. *Acc. Chem. Res.* **2013**, *46*, 1806–1815.

[32] Suntola, T.; Hyvarinen, J. Atomic layer epitaxy. *Annu. Rev. Mater. Sci.* **1985**, *15*, 177–195.

[33] Liu, J.; Liu, Y.; Liu, N. Y.; Han, Y. Z.; Zhang, X.; Huang, H.;

Lifshitz, Y.; Lee, S. T.; Zhong, J.; Kang, Z. H. Metal-free efficient photocatalyst for stable visible water splitting via a two-electron pathway. *Science* **2015**, *347*, 970–974.

[34] Han, Q.; Wang, B.; Gao, J.; Cheng, Z. H.; Zhao, Y.; Zhang, Z. P.; Qu, L. T. Atomically thin mesoporous nanomesh of graphitic C_3N_4 for high-efficiency photocatalytic hydrogen evolution. *ACS Nano* **2016**, *10*, 2745–2751.

[35] Lu, J. L.; Stair, P. C. Nano/subnanometer Pd nanoparticles on oxide supports synthesized by AB-type and low-temperature ABC-type atomic layer deposition: Growth and morphology. *Langmuir* **2010**, *26*, 16486–16495.

[36] Elam, J. W.; Zinovev, A.; Han, C. Y.; Wang, H. H.; Welp, U.; Hryn, J. N.; Pellin, M. J. Atomic layer deposition of palladium films on Al_2O_3 surfaces. *Thin Solid Films* **2006**, *515*, 1664–1673.

[37] Wang, H. W.; Wang, C. L.; Yan, H.; Yi, H.; Lu, J. L. Precisely-controlled synthesis of Au@Pd core–shell bimetallic catalyst via atomic layer deposition for selective oxidation of benzyl alcohol. *J. Catal.* **2015**, *324*, 59–68.

[38] Chen, B. R.; George, C.; Lin, Y. Y.; Hu, L. H.; Crosby, L.; Hu, X. Y.; Stair, P. C.; Marks, L. D.; Poeppelmeier, K. R.; Van Duyne, R. P. et al. Morphology and oxidation state of ALD-grown Pd nanoparticles on TiO_2- and SrO-terminated $SrTiO_3$ nanocuboids. *Surf. Sci.* **2016**, *648*, 291–298.

[39] Gao, G. P.; Jiao, Y.; Waclawik, E. R.; Du, A. J. Single atom (Pd/Pt) supported on graphitic carbon nitride as an efficient photocatalyst for visible-light reduction of carbon dioxide. *J. Am. Chem. Soc.* **2016**, *138*, 6292–6297.

[40] Lei, Y.; Lu, J.; Luo, X. Y.; Wu, T. P.; Du, P.; Zhang, X. Y.; Ren, Y.; Wen, J. G.; Miller, D. J.; Miller, J. T. et al. Synthesis of porous carbon supported palladium nanoparticle catalysts by atomic layer deposition: Application for rechargeable lithium-O_2 battery. *Nano Lett.* **2013**, *13*, 4182–4189.

[41] Gong, T.; Qin, L. J.; Zhang, W.; Wan, H.; Lu, J.; Feng, H. Activated carbon supported palladium nanoparticle catalysts synthesized by atomic layer deposition: Genesis and evolution of nanoparticles and tuning the particle size. *J. Phys. Chem. C* **2015**, *119*, 11544–11556.

[42] Zhou, W. J.; Lee, J. Y. Particle size effects in Pd-catalyzed electrooxidation of formic acid. *J. Phys. Chem. C* **2008**, *112*, 3789–3793.

[43] Tay, Q.; Kanhere, P.; Ng, C. F.; Chen, S.; Chakraborty, S.; Huan, A. C. H.; Sum, T. C.; Ahuja, R.; Chen, Z. Defect engineered g-C_3N_4 for efficient visible light photocatalytic hydrogen production. *Chem. Mater.* **2015**, *27*, 4930–4933.

[44] Zemlyanov, D.; Aszalos-Kiss, B.; Kleimenov, E.; Teschner, D.; Zafeiratos, S.; Hävecker, M.; Knop-Gericke, A.; Schlogl, R.; Gabasch, H.; Unterberger, W. et al. *In situ* XPS study of Pd(111) oxidation. Part 1: 2D oxide formation in 10^{-3} mbar O_2. *Surf. Sci.* **2006**, *600*, 983–994.

[45] Zhou, Y. K.; Pasquarelli, R.; Holme, T.; Berry, J.; Ginley, D.; O'Hayre, R. Improving PEM fuel cell catalyst activity and durability using nitrogen-doped carbon supports: Observations from model Pt/HOPG systems. *J. Mater. Chem.* **2009**, *19*, 7830–7838.

[46] Jia, L. J.; Bulushev, D. A.; Podyacheva, O. Y.; Boronin, A. I.; Kibis, L. S.; Gerasimov, E. Y.; Beloshapkin, S.; Seryak, I. A.; Ismagilov, Z. R.; Ross, J. R. H. Pt nanoclusters stabilized by N-doped carbon nanofibers for hydrogen production from formic acid. *J. Catal.* **2013**, *307*, 94–102.

[47] Wang, Q. J.; Che, J. G. Origins of distinctly different behaviors of Pd and Pt contacts on graphene. *Phys. Rev. Lett.* **2009**, *103*, 066802.

[48] Zhang, W. Y.; Huang, H. J.; Li, F.; Deng, K. M.; Wang, X. Palladium nanoparticles supported on graphitic carbon nitride-modified reduced graphene oxide as highly efficient catalysts for formic acid and methanol electrooxidation. *J. Mater. Chem. A* **2014**, *2*, 19084–19094.

[49] Noupa, C.; Rousset, J. L.; Tardy, B.; Bertolini, J. C. Sizeable deactivation effect for the 1,3-butadiene hydrogenation on vapor-deposited Pd aggregates on graphite. *Catal. Lett.* **1993**, *22*, 197–203.

[50] Silvestre-Albero, J.; Rupprechter, G.; Freund, H. J. Atmospheric pressure studies of selective 1,3-butadiene hydrogenation on well-defined Pd/Al_2O_3/NiAl(110) model catalysts: Effect of Pd particle size. *J. Catal.* **2006**, *240*, 58–65.

[51] Binder, A.; Seipenbusch, M.; Muhler, M.; Kasper, G. Kinetics and particle size effects in ethene hydrogenation over supported palladium catalysts at atmospheric pressure. *J. Catal.* **2009**, *268*, 150–155.

[52] Borodzinski, A.; Bond, G. C. Selective hydrogenation of ethyne in ethene-rich streams on palladium catalysts, Part 2: Steady-state kinetics and effects of palladium particle size, carbon monoxide, and promoters. *Catal. Rev.* **2008**, *50*, 379–469.

[53] Kang, J. H.; Shin, E. W.; Kim, W. J.; Park, J. D.; Moon, S. H. Selective hydrogenation of acetylene on TiO_2-added Pd catalysts. *J. Catal.* **2002**, *208*, 310–320.

[54] Sandell, A.; Beutler, A.; Jaworowski, A.; Wiklund, M.; Heister, K.; Nyholm, R.; Andersen, J. N. Adsorption of acetylene and hydrogen on Pd(111): Formation of a well-ordered ethylidyne overlayer. *Surf. Sci.* **1998**, *415*, 411–422.

[55] Borodziński, A. Hydrogenation of acetylene-ethylene mixtures on a commercial palladium catalyst. *Catal. Lett.* **1999**, *63*, 35–42.

[56] Ouyang, R. H.; Liu, J. X.; Li, W. X. Atomistic theory of ostwald ripening and disintegration of supported metal particles under reaction conditions. *J. Am. Chem. Soc.* **2013**, *135*, 1760–1771.